The Effect of Flood Protection Works on Flood Risk

Georgios Mitsopoulos [1] , **Michalis Diakakis** [2] , **Aristeides Bloutsos** [1] , **Efthymios Lekkas** [2] , **Evangelos Baltas** [3] **and Anastasios Stamou** [1,*]

1   Laboratory of Applied Hydraulics, Department of Water Resources and Environmental Engineering, National Technical University of Athens, 15773 Athens, Greece

2   Faculty of Geology and Geoenvironment, National and Kapodistrian University of Athens, 15784 Athens, Greece

3   Laboratory of Hydrology and Water Resources Development, Department of Water Resources and Environmental Engineering, National Technical University of Athens, 15773 Athens, Greece

*   Correspondence: stamou@mail.ntua.gr

Abstract: We pose the following research question: "what is the effect of flood protection works on flood risk?" To answer this question, we developed a flood risk assessment method that combines the typical hazard assessment via integrated hydrological and hydrodynamic calculations using HEC-HMS and 1D/2D HEC-RAS, respectively, and an original procedure for vulnerability assessment at the building level, which we applied in the town of Mandra in Attica, Greece. We performed calculations for 15 scenarios—combinations of return periods (T = 20, 50, 100, 150, and 200 y) and rain durations (t = 6, 12, and 18 h)—for the conditions of the year 2017, when there were no flood protection works, and today with these works in place. We identified the regions with high flood risk and concluded that the presence of the works caused a decrease in the inundation areas by 53–89%, along with reductions in the maximum water depths, the maximum flow velocities, and the average flood risk in Koropouli Street—the main street of Mandra, which suffered severe damage during the 2017 flood—by 38–62%, 18–52%, and 27–74%, respectively. The effect of the flood protection works increased with the increases in the return period and rain duration, while for the same return period the effect of the rain duration was more pronounced for the smaller return periods.

Keywords: flash floods; flood protection works; flood risk; flood vulnerability; HEC-RAS 1D/2D model; Mandra town (Attica)

1. Introduction

Between 1998 and 2009, Europe suffered over 213 major, damaging floods, including the catastrophic events along the Danube and Elbe rivers in the summer of 2002 [1]. Severe floods in 2005 further reinforced the need for concerted action. During the same period, floods in Europe caused some 1126 deaths, the displacement of about half a million people, and at least EUR 52 billion in insured economic losses [2], and even today catastrophic floods occur in parts of the continent, with disastrous results [3]. To reduce and manage the risks that floods pose to human health, the environment, cultural heritage, and economic activity, the European Commission proposed Directive 2007/60/EC on the assessment and management of flood risks (often referred to as the "Floods Directive" (FD)), which was published in the *Official Journal* in November 2007 [4]. According to the FD, "flood risk" is a function of the likelihood of a flood event together with the actual damage to human health and life, as well as the impacts on the environment and economic activities associated with that flood event. The quantification of flood risk is expressed either in monetary units or in loss of life units [5], if the losses are measurable, or in qualitative terms (e.g., allocation in classes) in the case of intangible damages (e.g., social, environment, cultural) to the affected areas [6]. The FD requires member states (1) to carry out a preliminary flood risk assessment (PFRA) to identify river basins that are areas of potentially significant flood risk (APSFRs) by 2011, (2) to draw up flood risk maps for these APSFRs by 2013, and (3) to establish

flood risk management plans focused on prevention [4] (i.e., preventing damage caused by floods by avoiding construction of houses and industries in present and future flood-prone areas), protection (i.e., taking measures—both structural and non-structural—to reduce the likelihood of floods and/or the impact of floods in a specific location), and preparedness (i.e., providing instructions and a code of conduct to the public on what to do in the event of flooding) by 2015 [4].

Flood risk assessment (FRA) is an interdisciplinary task [7] that combines various sources and types of information and models to estimate, a priori, what possible flood events may look like (i.e., flood extent and inundation depth), how probable they are, and what the possible consequences of such a flood may be [8]. Within the implementation of the FD, FRA follows the conceptual framework typically applied in engineering and natural sciences, where risk (R) incorporates the concepts of hazard (H) and vulnerability (V); in mathematical terms, this is expressed as $R = H \times V$ [3]. Flood hazard expresses the probability that a flood of a particular intensity will occur over periods ranging from years to decades, in order to support risk management activities [9]. Intensity usually refers to the combination of various hazard elements, including water depths, extent of flood inundation areas, flow velocities (to assess erosion and the collapse of buildings), and rates of water level rise (to assess potential fatalities and flood duration) [10]. Vulnerability is the degree of harm expected under certain conditions of exposure, susceptibility, and resilience [11]. Exposure refers to the presence of at-risk elements (e.g., people, buildings, services, infrastructure, or other properties) that could be adversely affected [12]; susceptibility is the likelihood of dangerous events occurring based on local conditions or as a result of the element's inherent inability to withstand the hazard impact [13]; while resilience is the ability of an at-risk element to anticipate, absorb or cope with, resist, and recover from the impact of a flood hazard [14]. To perform an FRA, firstly, flood hazard assessment (FHA) and flood vulnerability assessment (FVA) should be completed [15].

In the literature, there exist various approaches for flood hazard assessment (FHA) [16], which are influenced by a series of factors that can be divided into the following seven groups: hydrological and orographic, meteorological, geomorphological, cover characteristics, soil properties, infrastructure, and socioeconomic [17]; in practice, it is unclear how these factors affect one another and what their direct impact is on flood hazard [18]. FHA approaches are mainly quantitative and are often based on hydrological, hydrodynamic, or integrated hydrological–hydrodynamic modeling [19]; moreover, there are also qualitative methods that mainly rely on expert judgment [20]. FHA requires adequate observational data that can be based on recorded flood events; the latter are combined with time series of hydrological and hydrodynamic parameters, such as precipitation, river discharge, water depths, or water surface elevations, which can be used to derive the probabilities and corresponding magnitudes of possible flood events, e.g., via frequency analyses to derive return periods for certain surface water discharges/stages. FHA estimation within the FD requires the preparation of flood hazard maps for the APSFR according to the following scenarios: (a) floods with a low probability, or extreme event scenarios; (b) floods with a medium probability (likely return period (T) $\geq$ 100 years); and (c) floods with a high probability, where appropriate. For each scenario, the following hazard elements should be shown: (a) the extent of flooding, (b) the water depths or water elevations, and (c) the flow velocities or the relevant discharges. The approaches used in the calculation of return periods and probabilities by the 25 member countries include expert judgment, historical data, statistical analysis, modeling, hydrologic rainfall–runoff modeling, and hydrological studies [21]. Within the implementation of the FD in Greece, scenarios refer to T = 50, 100, and 1000 years, while flood hazard incorporates the hazard elements maximum water depth (D) and maximum water velocity (U) [22].

Usually, flood vulnerability assessment (FVA) refers to the assessment of susceptibility to damage to physical structures used for human shelter—which are mainly residential, commercial, or other buildings—as a result of flooding [23]. The term "damage" often refers to harm to the physical elements at risk, as well as the amount of resources needed

to restore the affected elements to their original function. Understanding, quantifying, and analyzing the vulnerability of physical properties is essential for designing strategies and adopting an approach for its reduction [24]. Flood damage can be assessed at a town scale or an object level [8], the latter of which is typically a building. Building-specific flood damage models can be developed using (a) flood loss data that can be collected immediately after a flood or (b) synthetic data that are derived following analyses by experts, surveys, or interviews [25]; these empirical and/or synthetic "damage data" can be combined with influencing parameters that include hydrodynamic (i.e., flood hazard) characteristics and resistance (i.e., vulnerability) characteristics. The popular methods for assessing physical flood vulnerability are vulnerability curves, vulnerability matrices, and indicator-based approaches [26]; the latter have the strength of allowing significant factors (e.g., building material, construction type, number of floors, level of maintenance, ground floor material) that contribute to flood vulnerability to be considered during FVA [13]. Within the implementation of the FD in Greece, the following five classes of vulnerability have been defined: very low, low, medium, important, and very important; these are based on a detailed analysis of the potential impacts of the flood—i.e., the degree of harm—on the following four categories of indicators: (1) population, (2) national economy, (3) environmental, and (4) cultural [22].

Once FRE is accomplished, flood risk management plans can be established focusing on reducing the flood risk via prevention, protection, and preparedness measures. Flood protection measures can be structural and non-structural. Structural measures refer to any physical construction to reduce or avoid the possible impacts of hazards, or the application of engineering techniques or technology to achieve hazard resistance and resilience in structures or systems [27]; they range from heavily engineered interventions (grey)—such as dams, reservoirs, embankments (e.g., levees, dykes) [28,29], bypass and diversion channels, and channelization—to more natural approaches (green or nature-based solutions), such as restoration of rivers and their floodplains and removal of embankments, planting of trees, floodplains or storage areas in the floodplain, and wooden leaky barriers or engineered logjams in rivers and/or floodplains [30]. Non-structural measures are measures not involving physical construction, which use knowledge, practice, or agreement to reduce disaster risks and impacts—in particular through policies and laws, raising public awareness, training, and education [27]; these include building awareness and mapping of hazard zones, better weather forecasting, better early-warning systems, education, preparedness exercises, hazard identification signs, land-use controls, building codes, and others [31].

Given the complexity and uncertainties of urban hydrology and hydraulics [32], it is important to know the effects of flood protection works on flood risk in urban environments, especially when faced with extreme flash floods. Thus, in the present paper, we pose the following research question: "What is the effect of flood protection works on flood risk?" To the best of our knowledge, there are no published works related to this question, despite its significant scientific and practical interest. To answer this question, we developed an FRA approach and applied it at the lowest possible (e.g., micro) spatial scale for the town of Mandra in Attica, Greece, based on calculations and data of the disastrous flash flood that occurred on 15 November 2017. The rest of this paper is organized as follows: In Section 2 "Materials and Methods", the area of study, the flood of 2017, the flood protection works, the scenarios of calculations, and the integrated modeling procedure are briefly described, and the proposed FRA approach is presented. In Sections 3 and 4, "Results and Discussion", the proposed FRA is applied to determine the flood risk for all scenarios in Mandra as it was during the flood in November 2017— i.e., effectively without flood protection works—and today with the works. In Section 5, we provide the "Conclusions".

2. Materials and Methods

2.1. The Area of Study, the Flood of 2017, and the Main Characteristics of the Flood Protection Works

The town of Mandra is situated in western Attica at the foothills of Mt. Pateras, whose hydrographic network consists of several converging creeks with steep slopes that form the streams (St) St Soures and St Agia Aikaterini that pass through the town of Mandra, as shown in Figure 1. The town, with a population of approximately 11,300 people, is situated at the boundary between Thriassion Plain to the east and Mt. Pateras to the west. Mandra is built approximately 3 km from the sea (Gulf of Eleusis) and 22 km from Athens—the capital of Greece—at the western boundary of the region of Attica. The plain has been home to extensive development in recent years, with numerous industrial units and small towns surrounding Mandra, exhibiting extensive socioeconomic activity. The western side of the study area is dominated by limestone rocks and characterized by sharp reliefs with steep slopes, due to the significant neotectonic activity [33]. In terms of hydrology, with the exception of rainy days, the river network is dry for most of the year. The town of Mandra is shaped by a relatively dense urban fabric, dominated by reinforced concrete buildings and asphalt streets, and can be considered a typical example of a modern-day urban landscape in the Eastern Mediterranean region. Mandra and its surroundings have the characteristics of a semi-arid area, with an annual rainfall close to 400 mm. However, its steep slopes and relatively small catchments (<30 km^2) [34] make it a flash-flood-prone area with a rich history of events in recent decades.

Figure 1. The area of study, the flood protection works, and the areas of interest.

In 2017, these streams were characterized by significant morphological changes due to the intensive construction activities in the greater area that resulted in a dramatic reduction in their available cross-sectional areas, which was one of the main reasons for the disaster

that occurred on 15 November 2017 [35]. The flash flood was estimated to correspond to a return period equal to approximately 150 years; most of the population was affected by the flood (24 deaths and 24 people injured), while basements and ground floors of buildings in the town were seriously damaged, along with severe impacts on infrastructure, vehicles, and the environment [34]. Officials estimated that 80% of the town area had been affected [36]. Due to this catastrophic event, the Greek Government immediately decided to construct flood protection works in Mandra based on their Final Study performed in 2014 for a design flood with a return period equal to 50 years, which was based on rainfall curves determined from a hydrological study performed in 1980. Moreover, in October 2019, the design of an exemplary early-warning system for floods in Mandra [37] was performed within the project CLIMPACT [38]. The construction of the flood protection works started in 2018 and was completed by July 2021; these works mainly included the following (see Figure 1): (1) the regulation of St Soures for a length of 1780 m, for a design flow equal to 91 m^3/s (x = 239–1780 m) and 125 m^3/s (x = 0–239 m); and (2) the diversion of St Agia Aikaterini to St Soures via a 1451 m long channel for a design flow equal to 47 m^3/s. A more detailed description of the flood protection works can be found in the work of Stamou et al. [39].

In this work, the main areas of interest are the residential area and the industrial area in the town of Mandra. In the residential area, our attention is focused on Koropouli Street, which is the main street of the town of Mandra and suffered severe flooding during the flash flood of November 2017; the axis of Koropouli Street is shown in Figure 1 (noted as Koropouli conduit).

2.2. Scenarios of Calculations

Calculations were performed with and without the flood protection works for 15 combinations of values of return period (T = 20, 50, 100, 150, and 200 y) and rain duration (t = 6, 12, and 18 h), for a total of 30 scenarios, as shown in Table 1.

Table 1. Scenarios of calculations.

Flood Protection Works	No					Yes				
T(y)	20	50	100	150	200	20	50	100	150	200
t = 6 h	S20-06	S50-06	S100-06	S150-06	S200-06	W20-06	W50-06	W100-06	W150-06	W200-06
t = 12 h	S20-12	S50-12	S100-12	S150-12	S200-12	W20-12	W50-12	W100-12	W150-12	W200-12
t = 18 h	S20-18	S50-18	S100-18	S150-18	S200-18	W20-18	W50-18	W100-18	W150-18	W200-18

2.3. Hydrological and Hydrodynamic Modeling

The proposed FRA approach involves the use of an integrated modeling procedure that combines the hydrological model HEC-HMS [40] and the HEC-RAS 1D/2D model [41]. The hydrological analysis was conducted with the aid of the Hydrologic Modeling System (HEC-HMS) in order to incorporate and combine different methods concerning the rainfall–runoff transformation, the hydrological losses, and the river routing and, finally, to generate the flood hydrograph. The hydrological analysis output was then used in the River Analysis System (HEC-RAS), which has the ability to model unsteady flow through a river channel network and produce the water profiles, velocity, and inundation maps of the flood plain. Furthermore, two approaches—the GIS-based time–area diagram and the NRCS (SCS) Synthetic Curvilinear Dimensionless Unit Hydrograph—were employed. When effective rainfall was used as the input, the Soil Conservation Service Curve Number (SCS-CN) procedure was applied for estimation of hydrological losses based on the available total rainfall data [40]. The rainfall input was estimated for different periods based on intensity–duration–frequency (IDF) curves for the area [42,43]. HEC-RAS 1D/2D combines 1D modeling in the cross-sections of the two main streams in Mandra with 2D modeling in

the rest of the potentially flooded area of the computational domain. The coupled 1D and 2D solution algorithm allows for direct feedback in each computation step between 1D and 2D flow fields [41].

The produced hydrographs and the corresponding peak discharges are shown in Figure 2 and Table 2, respectively.
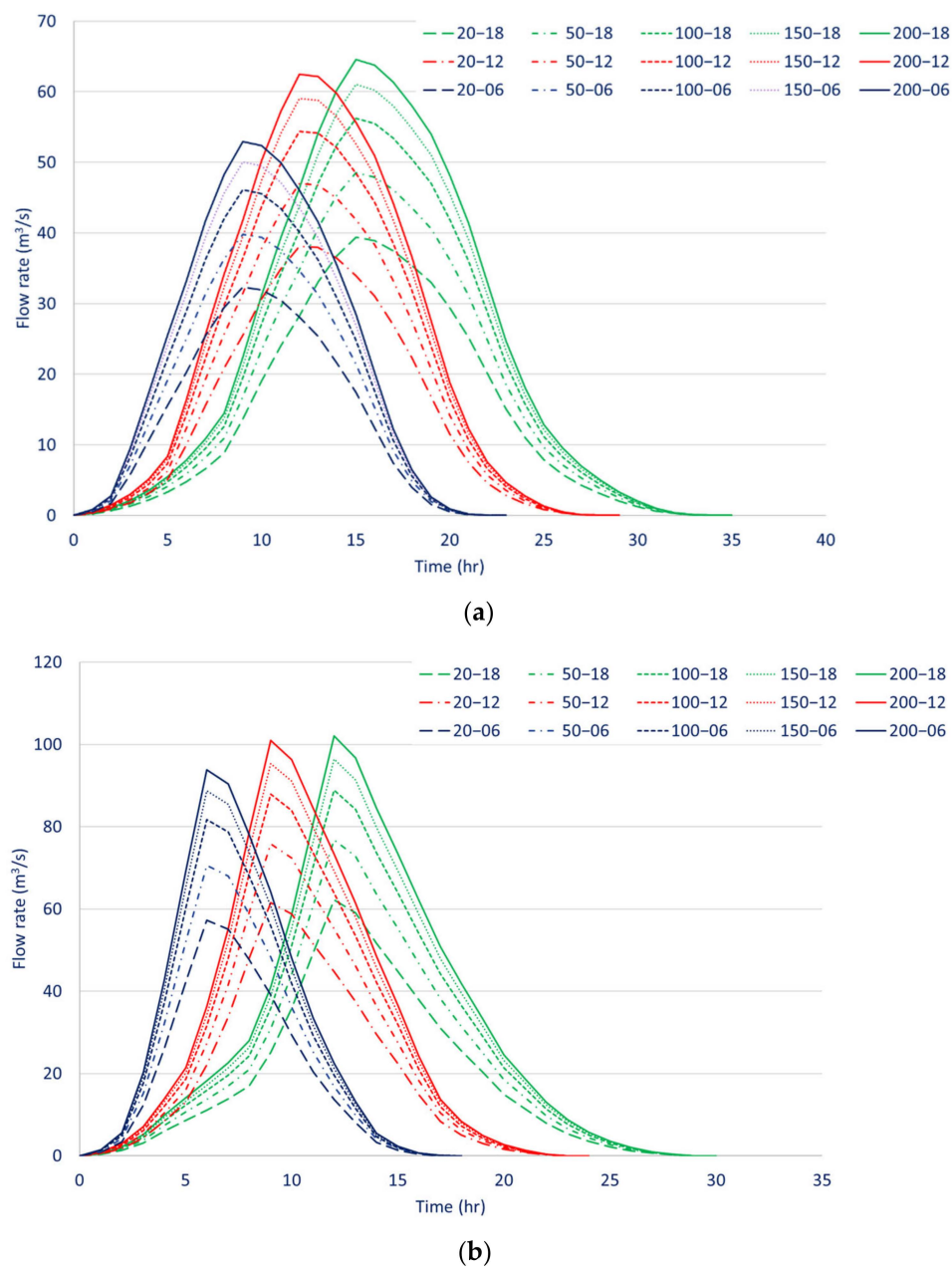

(a)

(b)

Figure 2. Calculated discharge hydrographs for (**a**) St Soures and (**b**) St Agia Aikaterini.

Table 2. Peak flow rates.

	T (y)—St Soures					T (y)—St Agia Aikaterini				
t (h)	20	50	100	150	200	20	50	100	150	200
6	32.31	39.82	46.11	50.04	52.96	57.27	70.59	81.72	88.7	93.86
12	38.13	46.99	54.41	59.05	62.49	58.77	75.88	87.85	95.35	100.9
18	39.39	48.55	56.21	61.00	64.56	62.26	76.73	88.83	96.41	102.03

The main input data for the hydrodynamic model were (i) the digital surface model (DSM) with a very high resolution equal to 0.80 m × 0.80 m, capturing all hydraulically important features of the area's surface—including streets, trees, and buildings—that are required for detailed hydrodynamic calculations; (ii) the distribution of the Manning roughness coefficient values in the computational domain; and (iii) the input hydrographs of the two streams as their upstream boundary conditions (see Figure 2). A detailed description of the calibration procedure of the hydrodynamic model and more information on the hydrodynamic calculations can be found in [28].

2.4. Flood Risk Assessment Approach

In the proposed FRA, flood hazard follows the approach of the implementation of the FD in Greece, i.e., 5 classes of flood hazard are defined, which are calculated based on Table 3 using the elements maximum water depth (D) and maximum water velocity (U) as inputs, which correspond to the 5 hazard scores (H = 0.2, 0.4, 0.6, 0.8 and 1.0) quoted in parentheses; these scores can be considered as flood probabilities.

Table 3. Flood hazard classes.

D (m)	U (m/s)			
	<0.5	**0.5–2.0**	**2.0–4.0**	**>4.0**
<0.2	Very Low (0.2)	Very Low (0.2)	Very Low (0.2)	Low (0.4)
0.2–0.5	Low (0.4)	Low (0.4)	Medium (0.6)	Medium (0.6)
0.5–1.0	Low (0.4)	Medium (0.6)	High (0.8)	High (0.8)
1.0–1.5	Medium (0.6)	Medium (0.6)	High (0.8)	Very high (1.0)
1.5–2.0	High (0.8)	High (0.8)	Very high (1.0)	Very high (1.0)
>2.0	Very high (1.0)	Very high (1.0)	Very high (1.0)	Very high (1.0)

Susceptibility to flood damage was assessed at a town (i.e., micro) scale using the object "building" via a 4-step procedure that enabled us (a) to better differentiate generic classes of buildings (e.g., between types of houses), as there is less heterogeneity in these classes; and (b) to perform site visits and individual inspections to specify or improve the damage curves [44]. As a first step, a field survey was performed to record specific characteristics for each building examined, including light wells, underground garage doors, pilotis, numbers of adjacent structures, the buildings' lowest openings (such as doors and windows), and their elevation relative to the surrounding area. In the second step, the recorded building characteristics were connected to the probability of a building experiencing internal flooding through statistically significant relationships, while in the third step a score of this probability was determined based on the presence of these building parameters and their respective weights denoting their influence. The fourth step divided the buildings in 5 classes of vulnerability (V), ranging from 0.2 (very low) to 1.0 (very high).

To estimate vulnerability on an individual building basis, we collected and exploited data on building characteristics, using features that have been associated with structures' susceptibility to flooding in the literature [45–50]. To this end, we used statistical associations documented by Diakakis et al. [51] for buildings in Greece, which connected specific external characteristics (i.e., light wells, underground garage doors, pilotis, numbers of adjacent structures, buildings' lowest openings (such as doors and windows), and their elevation relative to the surrounding area) with the impact of a flood on the building. This association is given by the following equation [51]:

$$Y = 1.372 + 1.143LW + 1.124UGR + 1.031PLT1 + 0.900PLT2 + 1.231BLO1 + 1.155BLO2 - 0.838ADJ1 \tag{1}$$

where LW, UGR, PLT1, PLT2, BLO1, BLO2, and ADJ1 are independent variables representing distinct building characteristics, as shown in Table 4.

Table 4. Description of independent variables representing building characteristics.

Independent Variable	Description
LW	Light well (Cour anglaise)
UGR	Garage ramps leading to underground spaces
PLT1 and PLT2	Pillars (pilotis) and their relevant position; PLT1 denotes pilotis below ground level and PLT2 denotes pilotis at ground level
BLO1 and BLO2	Relevant position of the buildings' lower openings (windows or doors); BLO1 denotes openings below ground level and BLO2 denotes openings at ground level
ADJ1	Adjacency to other buildings (measured as the number of sides exposed to open space); in this case, ADJ1 denotes 1 open side.

The dependent variable (Y) of binary logistic regression is connected with the estimated probability (p) of the flood's binary outcome via Equation (2), which can be reformed into Equation (3):

$$Y = \ln (p/1 - p) \tag{2}$$

$$p = \exp(Y)/(\exp(Y) + 1) \tag{3}$$

Using Equation (3) and substituting the dependent variable (Y) using Equation (1), we connected the independent variables (i.e., building characteristics) with the probability of internal flooding. This probability (p) was used as a proxy indicator of vulnerability for each building, with values ranging from 0 to 1. The probability of internal flooding was also chosen as a measure of vulnerability to address the uncertainty inherent in risk assessment [28,52]

For cartographic purposes, we grouped probability (p) values into 5 categories: 0 to 0.2, 0.2 to 0.4, 0.4 to 0.6, 0.6 to 0.8, and 0.8 to 1.0. Risk was calculated as R = H × V [3].

3. Results

3.1. Calculated Inundation Area

Inundation areas were calculated for all scenarios and are shown in Figure 3; these ranged from 0.10 to 2.14 km^2. Indicatively, the inundation areas for scenarios S20-06, W20-06, S200-18, and W200-18 are shown in Figure 4. Moreover, Table 5 depicts the effect of the flood protection works (%) on the inundation area.

Table 5. Reduction in the inundation area (%) because of the flood protection works.

T(y)	20	50	100	150	200
t = 6 h	93	77	69	61	56
t = 12 h	89	73	62	56	54
t = 18 h	89	73	62	55	53

Based on Figures 3 and 4, as well as Table 5, the following remarks can be made:

1. The inundation areas range from 1.45 to 2.14 km^2 without works for the extreme scenarios S20-06 and S200-18, and from 0.10 to 1.00 km^2 with works for the extreme scenarios W20-06 to W200-18. The inundation area increases with increasing return period and increasing rain duration.

2. The effect of the works on the inundation areas is very pronounced. The presence of the works results in a decrease in the inundation areas by 53–89%. As expected, this reduction decreases with increasing return period, while for the same return period the effect of the rain duration is more pronounced for the smaller return periods.
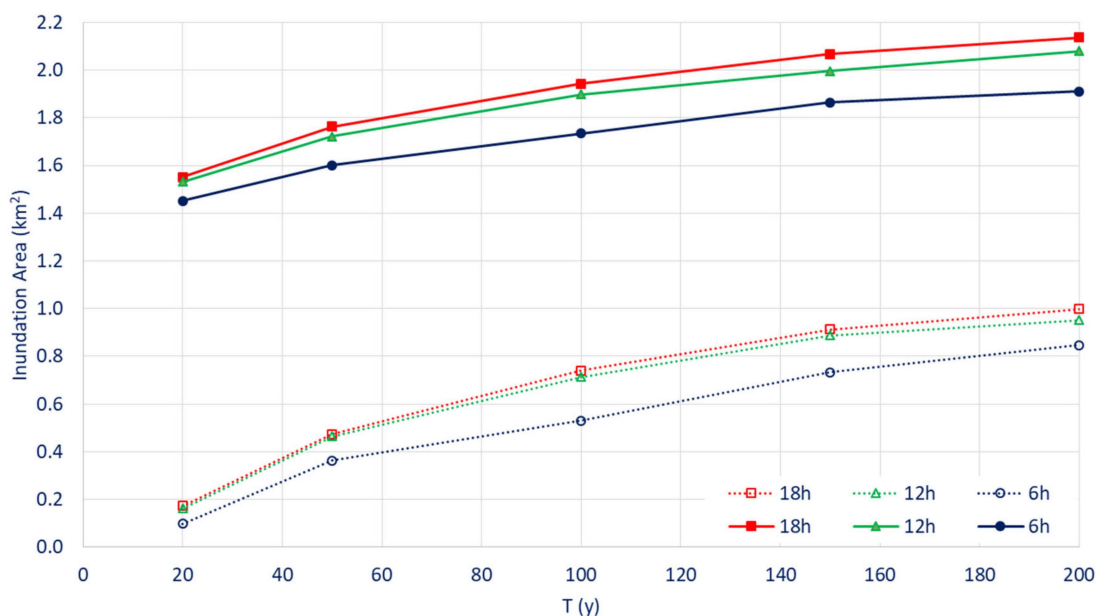
Figure 3. Calculated inundation areas for all scenarios (dotted lines refer to scenarios with flood protection works).

3.2. Flood Hazard Assessment

Figures 5 and 6 show the calculated maximum water depths and flow velocities, respectively, for scenarios S20-06, W20-06, S200-18, and W200-18, while Figures 7 and 8 show the distribution of the calculated maximum water depth and maximum flow velocity along Koropouli Street for the same scenarios, respectively. In Figures 9 and 10, the calculated flood hazards are shown in the residential and the industrial area, respectively, for four indicative scenarios. In Figure 11, the distribution of the calculated flood hazard along Koropouli Street is shown for four indicative scenarios, while Tables 6 and 7 show the average hazard values along Koropouli Street for all scenarios and their reduction because of the flood protection works, respectively.

Table 6. Average hazard on Koropouli Street.

Flood Protection Works	No	Yes	No	Yes	No	Yes	No	Yes	No	Yes
T(y)	20	20	50	50	100	100	150	150	200	200
t = 6 h	0.75	0.19	0.79	0.33	0.82	0.47	0.83	0.58	0.85	0.62
t = 12 h	0.77	0.24	0.80	0.37	0.83	0.57	0.85	0.63	0.86	0.65
t = 18 h	0.77	0.24	0.80	0.37	0.83	0.58	0.85	0.64	0.86	0.65

Table 7. Reduction in the average hazard (%) on Koropouli Street due to the presence of the flood protection works.

T(y)	20	50	100	150	200
t = 6 h	75	58	43	30	27
t = 12 h	69	54	31	27	24
t = 18 h	68	54	31	25	24

(a)

(b)

Figure 4. Inundation area for 4 indicative scenarios: (**a**) Scenarios S20-06 (**left**) and W20-06 (**right**) for T = 20 y and t = 6 h. (**b**) Scenarios S200-18 (**left**) and W200-18 (**right**) for T = 200 y and t = 18 h.
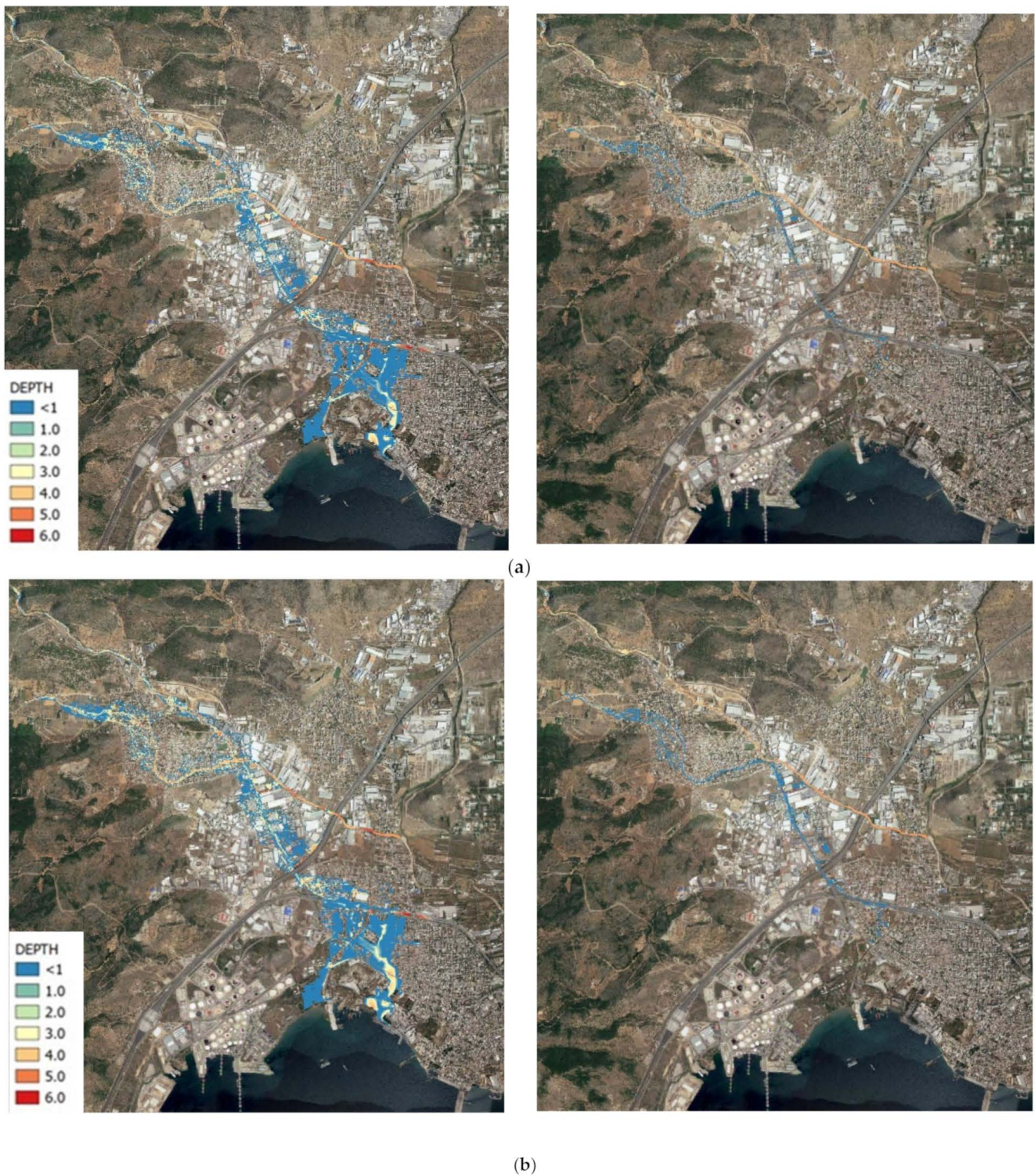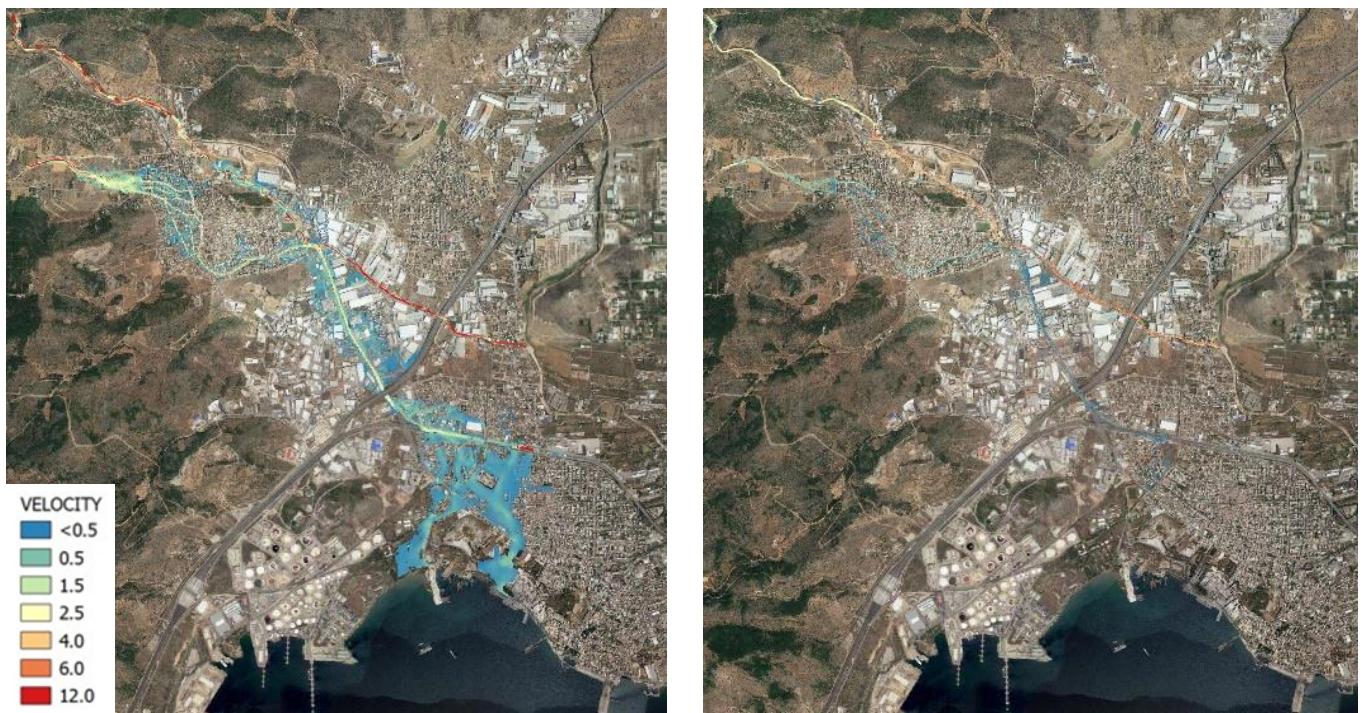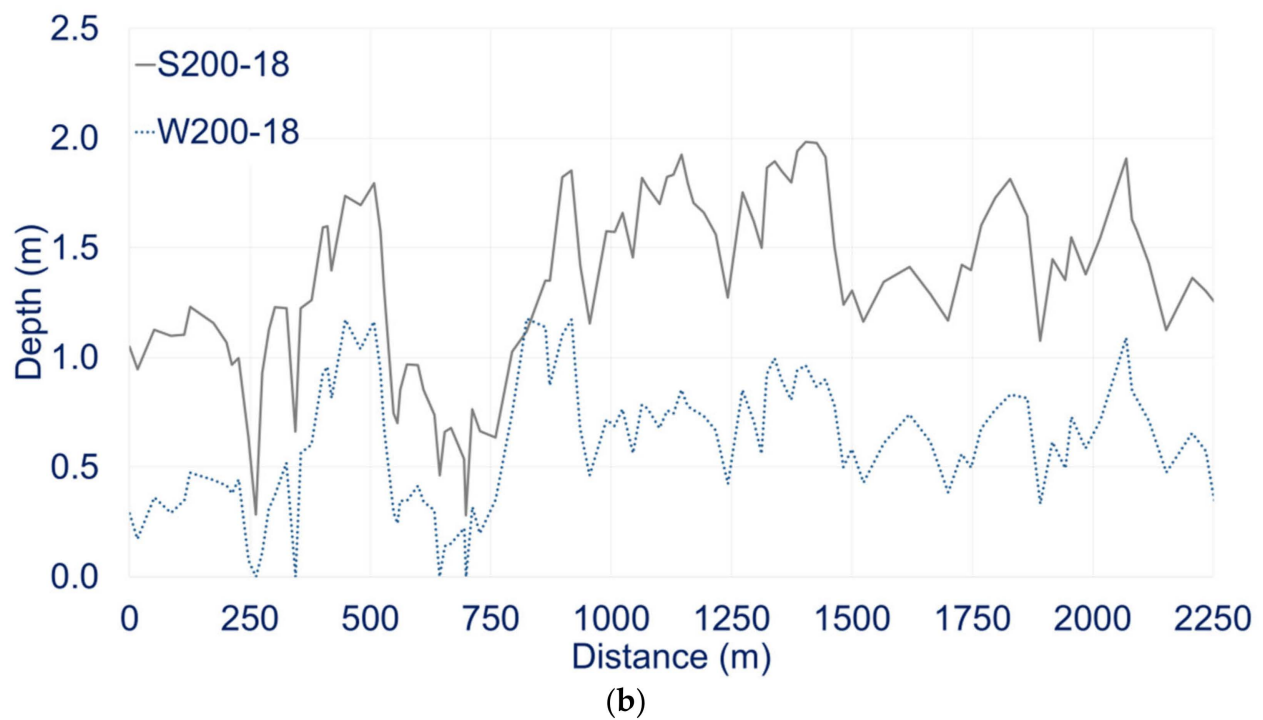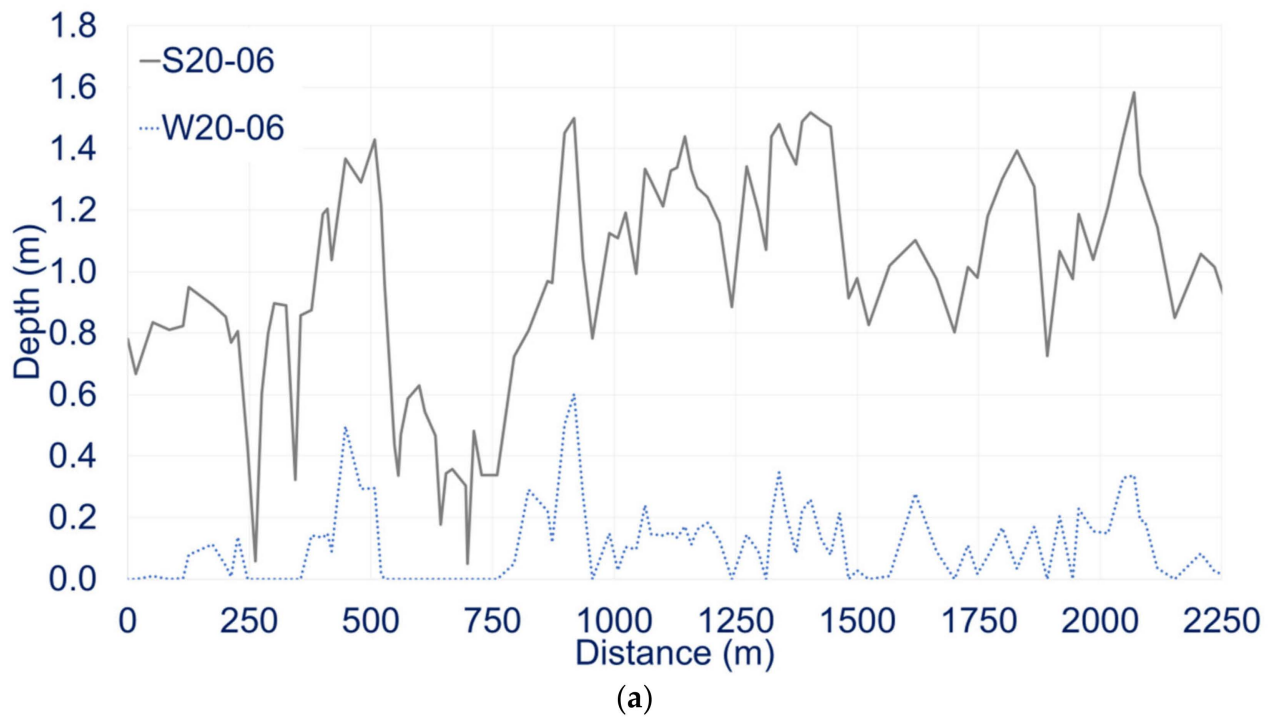
(a)

(b)

Figure 5. Maximum water depths (m) for 4 indicative scenarios: (**a**) Scenarios S20-06 (**left**) and W20-06 (**right**) for T = 20 y and t = 6 h. (**b**) Scenarios S200-18 (**left**) and W200-18 (**right**) for T = 200 y and t = 18 h.

(**a**)

(**b**)

Figure 6. Maximum water velocities (m/s) for 4 indicative scenarios: (**a**) Scenarios S20-06 (**left**) and W20-06 (**right**) for T = 20 y and t = 6 h. (**b**) Scenarios S200-18 (**left**) and W200-18 (**right**) for T = 200 y and t = 18 h.

(a)

(b)

Figure 7. Maximum water depth along Koropouli Street for 4 indicative scenarios: (**a**) Scenarios S20-06 and W20-06 for T = 20 y and t = 6 h. (**b**) Scenarios S200-06 and W200-06 for T = 200 y and t = 18 h.
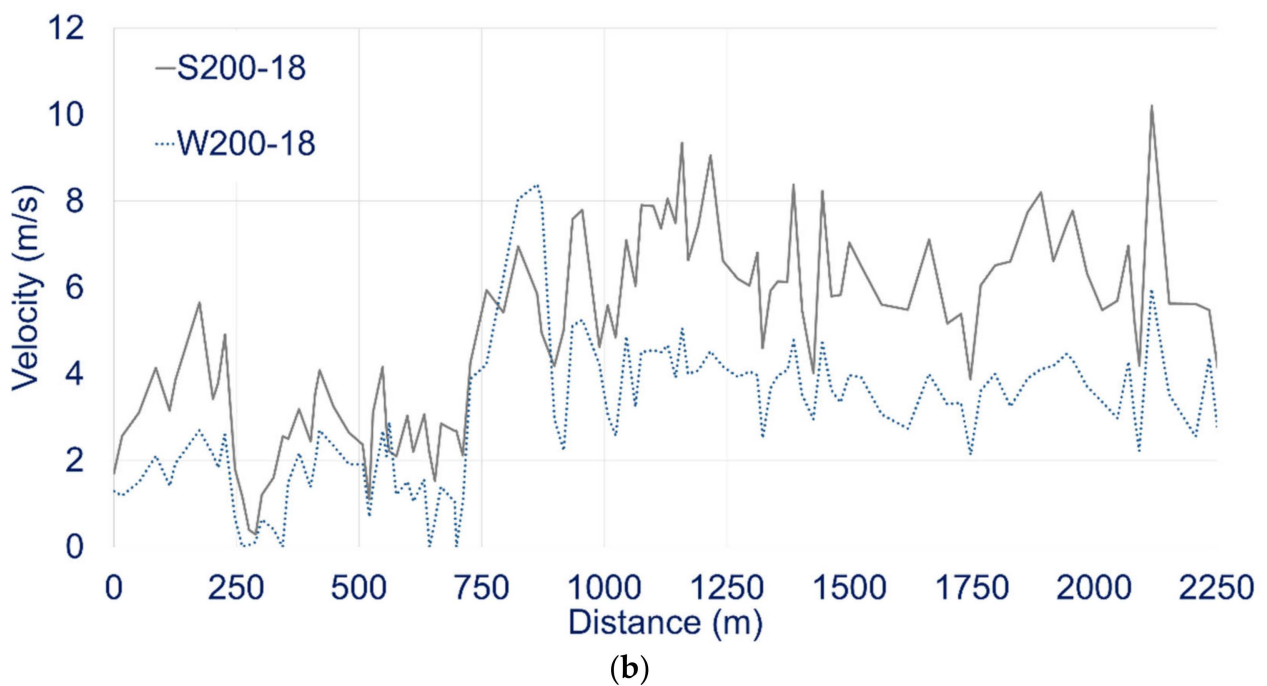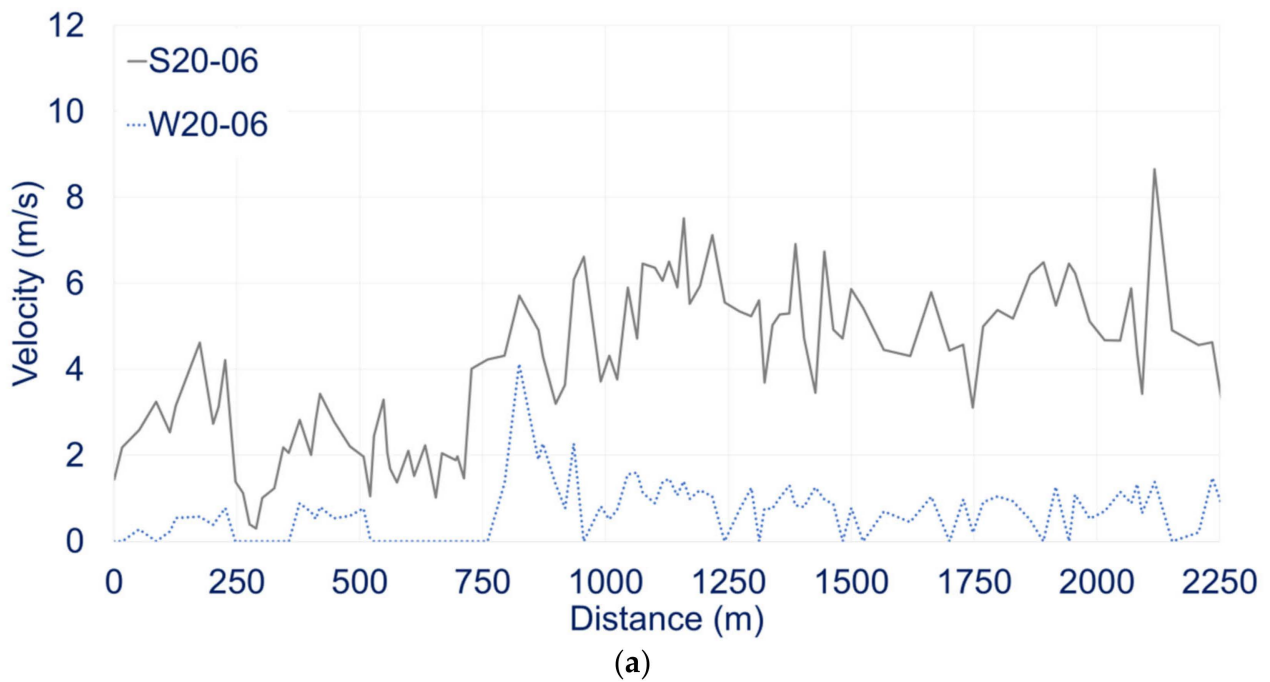
Figure 8. Maximum water velocity along Koropouli Street for 4 indicative scenarios: (**a**) Scenarios S20-06 and W20-06 for T = 20 y and t = 6 h. (**b**) Scenarios S200-06 and W200-06 for T = 200 y and t = 18 h.
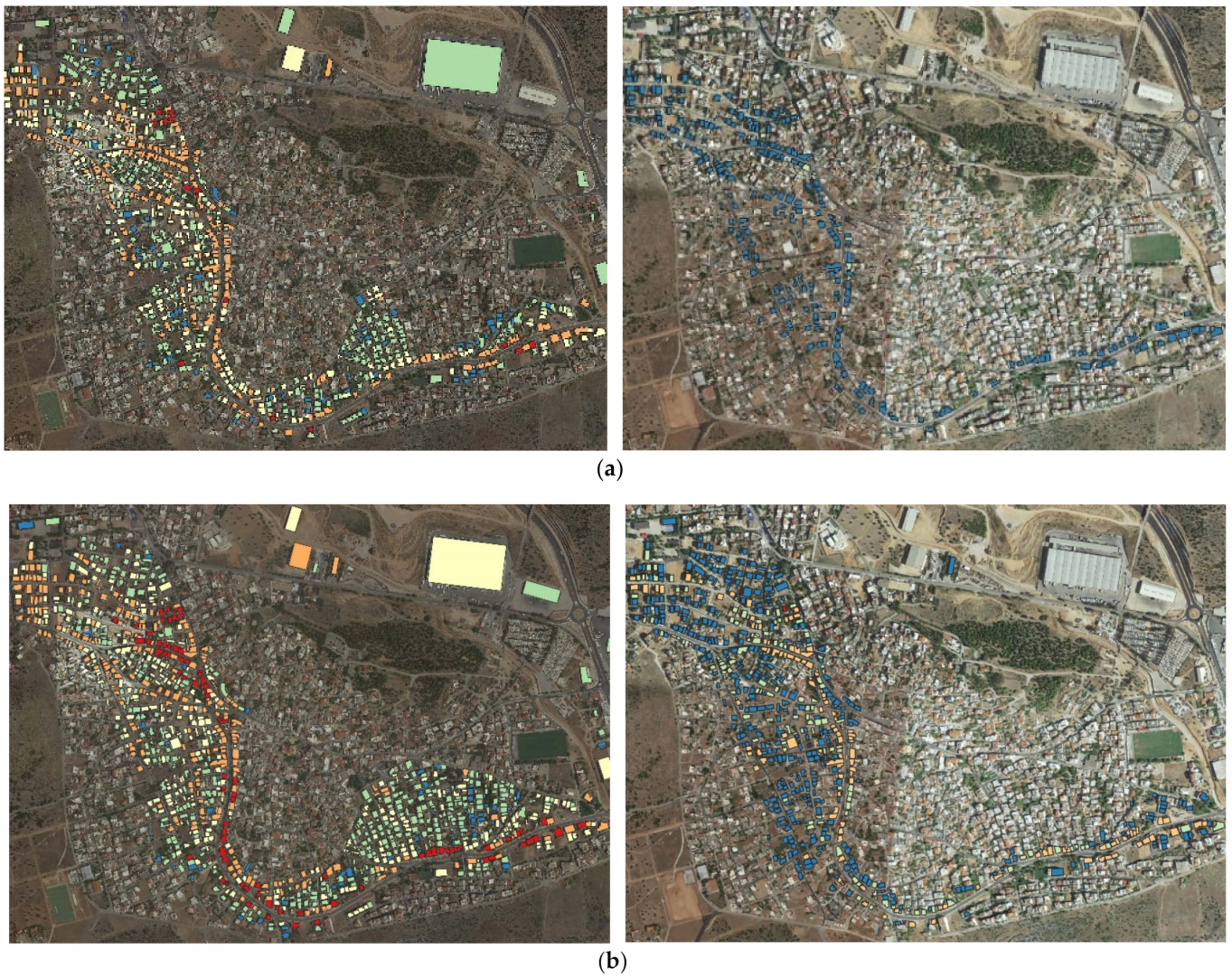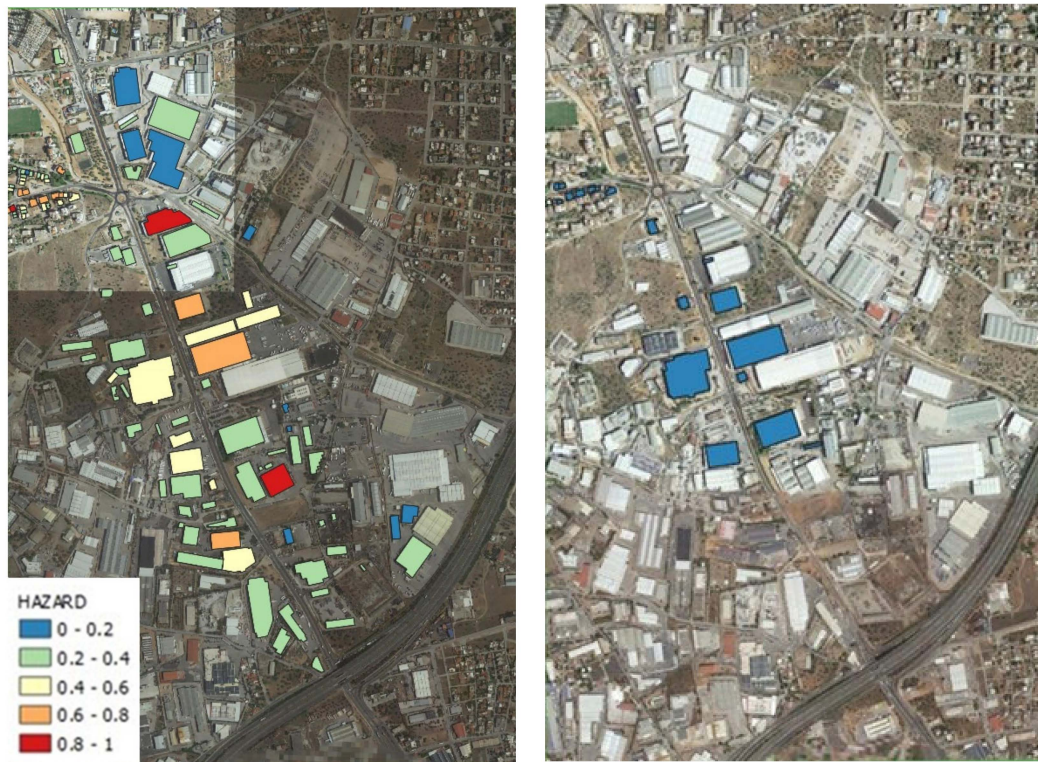
(**a**)

(**b**)

Figure 9. Flood hazard (H) in the residential area for 4 indicative scenarios: (**a**) Scenarios S20-06 (**left**) and W20-06 (**right**) for T = 20 y and t = 6 h. (**b**) Scenarios S200-18 (**left**) and W200-18 (**right**) for T = 200 y and t = 18 h.

(**a**)

(**b**)

Figure 10. Flood hazard (H) in the industrial area for 4 indicative scenarios: (**a**) Scenarios S20-06 (**left**) and W20-06 (**right**) for T = 20 y and t = 6 h. (**b**) Scenarios S200-18 (**left**) and W200-18 (**right**) for T = 200 y and t = 18 h.
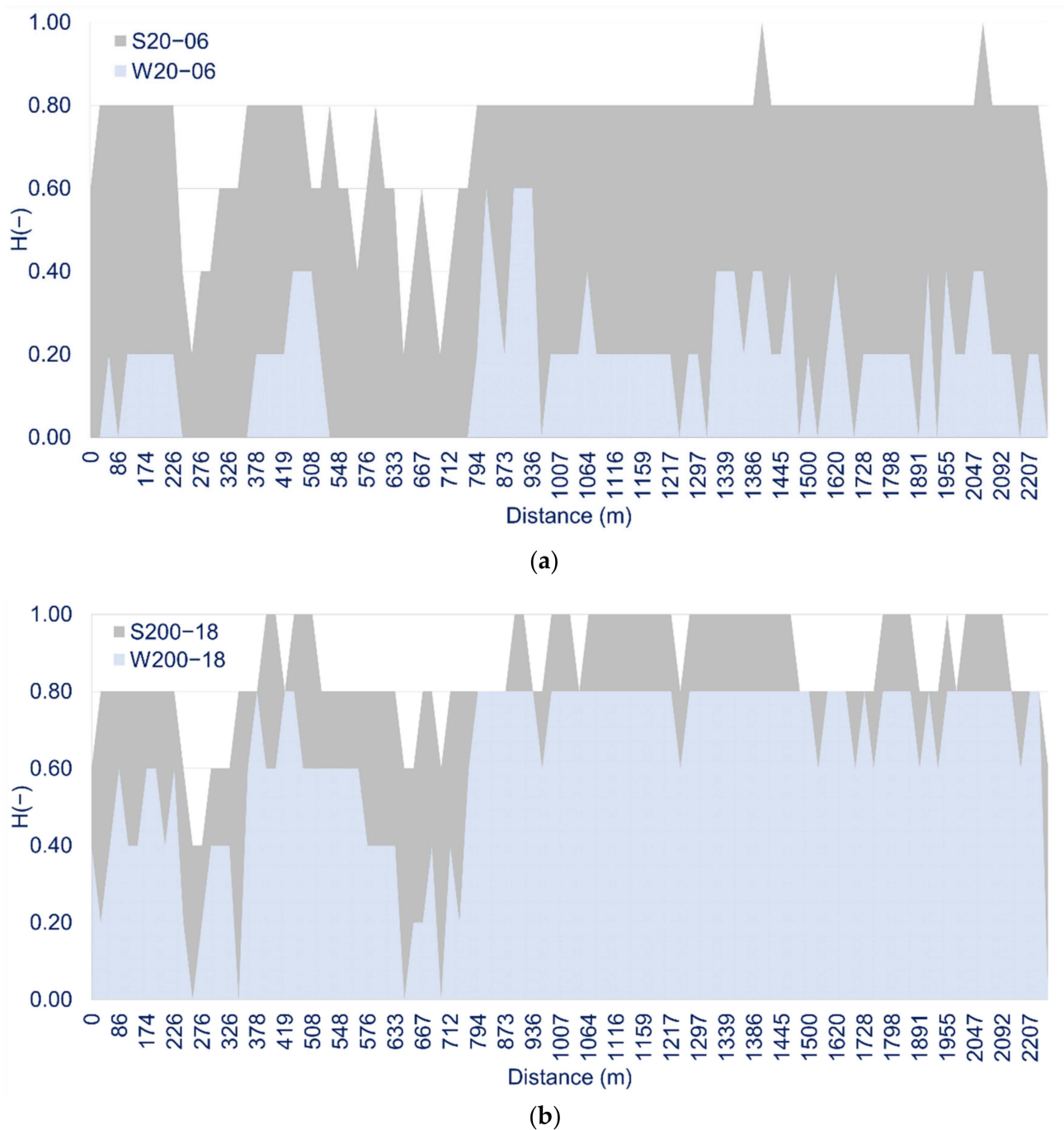
(a)

(b)

Figure 11. Calculated flood hazard (H) along Koropouli Street for 4 indicative scenarios: (**a**) Scenarios S20-06 and W20-06 for T = 20 y and t = 6 h. (**b**) Scenarios S200-18 and W200-18 for T = 200 y and t = 18 h.

Based on Figures 5–11 and Tables 6 and 7, the following remarks can be made:

1. Along Koropouli Street, the maximum water depths range from 1.58 to 1.98 m for the extreme scenarios S20-06 and S200-18 (without works), respectively, and from 0.60 to 1.18 m for the extreme scenarios W20-06 and W200-18 (with works), respectively. The maximum flow velocities range from 8.66 to 10.21 m/s for the extreme scenarios S20-06 and S200-18 (without works), respectively, and from 4.13 to 8.40 m/s for the extreme scenarios W20-06 and W200-18 (with works), respectively. The maximum water depths and flow velocities increase with increasing return period and increasing rain duration. The effect of the flood protection works on the maximum water depths

is significant. The presence of the works reduces the maximum water depths by 38–62% and the maximum flow velocities by 18–52%; the maximum reductions are observed for the minimum return period and maximum rain duration.

2. The maximum flood hazard values in the residential area range from 0.80 to 1.00 m for the extreme scenarios S20-06 and S200-18 (without works), respectively, and from 0.60 to 0.80 m for the extreme scenarios W20-06 and W200-18 (with works), respectively. Following the behavior of the maximum water depths and flow velocities, the flood hazard increases with increasing return period and increasing rain duration. Moreover, the effect of the flood protection works on the average flood hazard along Koropouli Street is pronounced; the average value of hazard ranges from 0.75 to 0.78 for the extreme scenarios S20-06 and S200-18, respectively, and from 0.19 to 0.65 for the extreme scenarios W20-06 and W200-18, respectively. In other words, the presence of the works results in a decrease in the flood hazard by 24–75%; as expected, this reduction decreases with increasing return period and decreasing rain duration. It should be noted that this dependence on the rain duration becomes weaker with longer rain durations.

3.3. Vulnerability Assessment

Figure 12 illustrates the probability of internal flooding as a proxy indicator of the building's flood vulnerability in five classes, with values ranging from 0 to 1.0. In total, vulnerability assessment was applied to 1462 buildings, covering constructions within the floodplain at this segment of the streams. Overall, in the examined sample, the values ranged from 0.099 to 0.893, with a mean value of 0.368 (standard deviation = 0.176). The higher vulnerability values were observed mostly for buildings with belowground openings—especially underground garage ramps/doors. There were no particular spatial patterns identified, apart from a small patch of low vulnerability in the oldest part of the town, where belowground openings were almost entirely absent. The majority of the buildings belonged to the second (light green) and third (yellow) vulnerability classes, whereas only a few were found to belong to categories four (orange) and five (red) (Figure 12).

3.4. Risk Assessment

Figures 13 and 14 show the calculated risk for the scenarios S20-06, W20-06, S200-18, and W200-18 in the residential area and the industrial area, respectively, while Figure 15 shows the relationship between the average risk and the flood return period. Based on Figures 13–16 and Tables 8 and 9, the following remarks can be made:

1. The maximum flood risk values in the residential area range from 0.73 to 0.86 for the extreme scenarios S20-06 and S200-18 (without works), respectively, and from 0.46 to 0.59 for the extreme scenarios W20-06 and W200-18 (with works), respectively. The flood risk increases with increasing return period and increasing rain duration.

2. The effect of the flood protection works on the average flood risk along Koropouli Street is pronounced; the average value of risk ranges from 0.28 to 0.32 for the extreme scenarios S20-06 and S200-18, respectively, and from 0.07 to 0.23 for the extreme scenarios W20-06 and W200-18, respectively, i.e., the presence of the works results in a decrease in the flood risk by 27–74%. This reduction decreases with increasing return period and decreasing rain duration; moreover, its dependence on the rain duration becomes very small with longer rain durations.

Figure 12. Calculated building vulnerability grouped in 5 classes.

Table 8. Average value of risk on Koropouli Street.

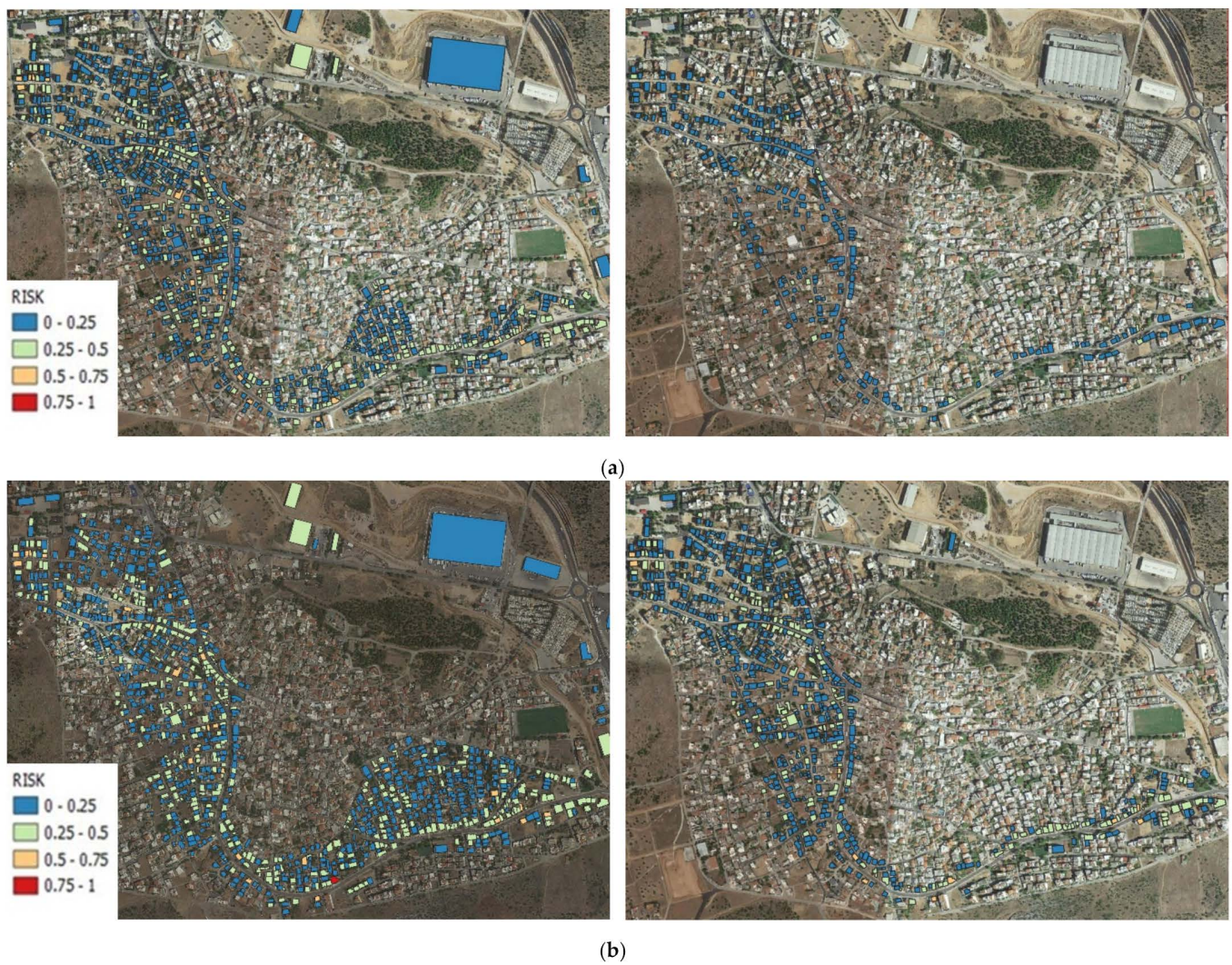| Flood Protection Works	No	Yes	No	Yes	No	Yes	No	Yes	No	Yes
T(y)	20	20	50	50	100	100	150	150	200	200
t = 6 h	0.28	0.07	0.28	0.12	0.29	0.16	0.30	0.19	0.31	0.21
t = 12 h	0.28	0.10	0.29	0.13	0.30	0.19	0.31	0.22	0.31	0.23
t = 18 h	0.28	0.10	0.29	0.13	0.30	0.19	0.31	0.22	0.32	0.23

(**a**)

(**b**)

Figure 13. Flood risk in the residential area for 4 indicative scenarios: (**a**) Scenarios S20-06 (**left**) and W20-06 (**right**) for T = 20 y and t = 6 h. (**b**) Scenarios S200-18 (**left**) and W200-18 (**right**) for T = 200 y and t = 18 h.

Table 9. Reduction in the risk (%) on Koropouli Street due to the presence of the flood protection works.

T(y)	20	50	100	150	200
t = 6 h	74	58	46	36	32
t = 12 h	66	56	37	30	27
t = 18 h	66	56	36	29	27
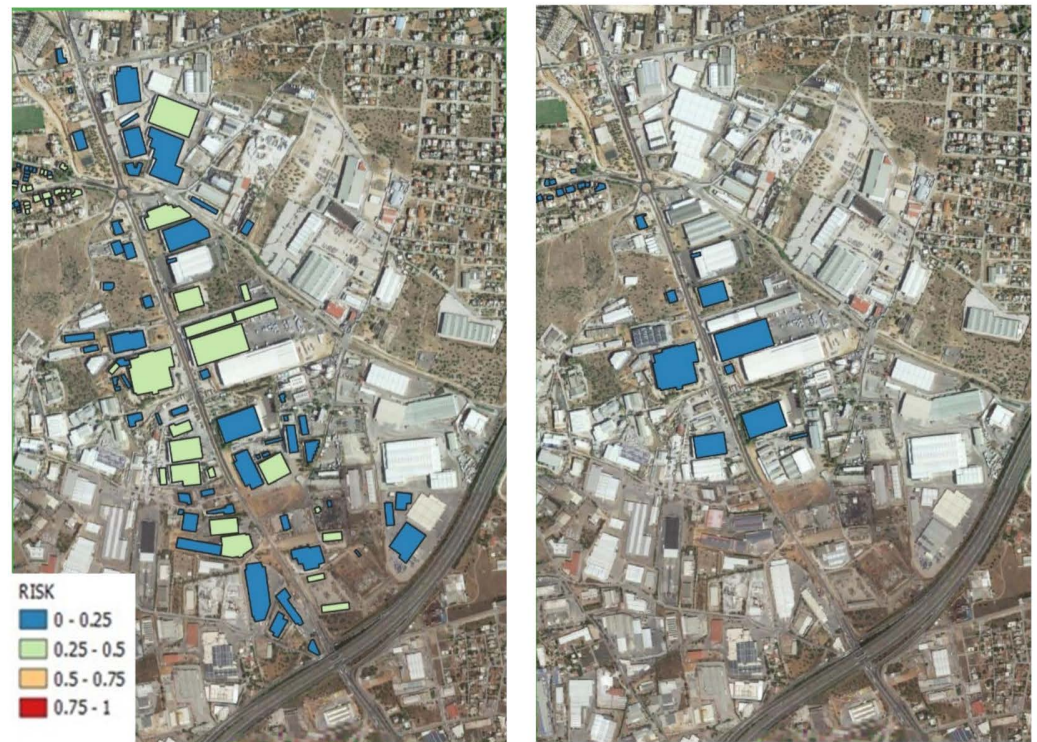
(**a**)

(**b**)

Figure 14. Flood risk in the industrial area for 4 indicative scenarios: (**a**) Scenarios S20-06 (**left**) and W20-06 (**right**) for T = 20 y and t = 6 h. (**b**) Scenarios S200-18 (**left**) and W200-18 (**right**) for T = 200 y and t = 18 h.
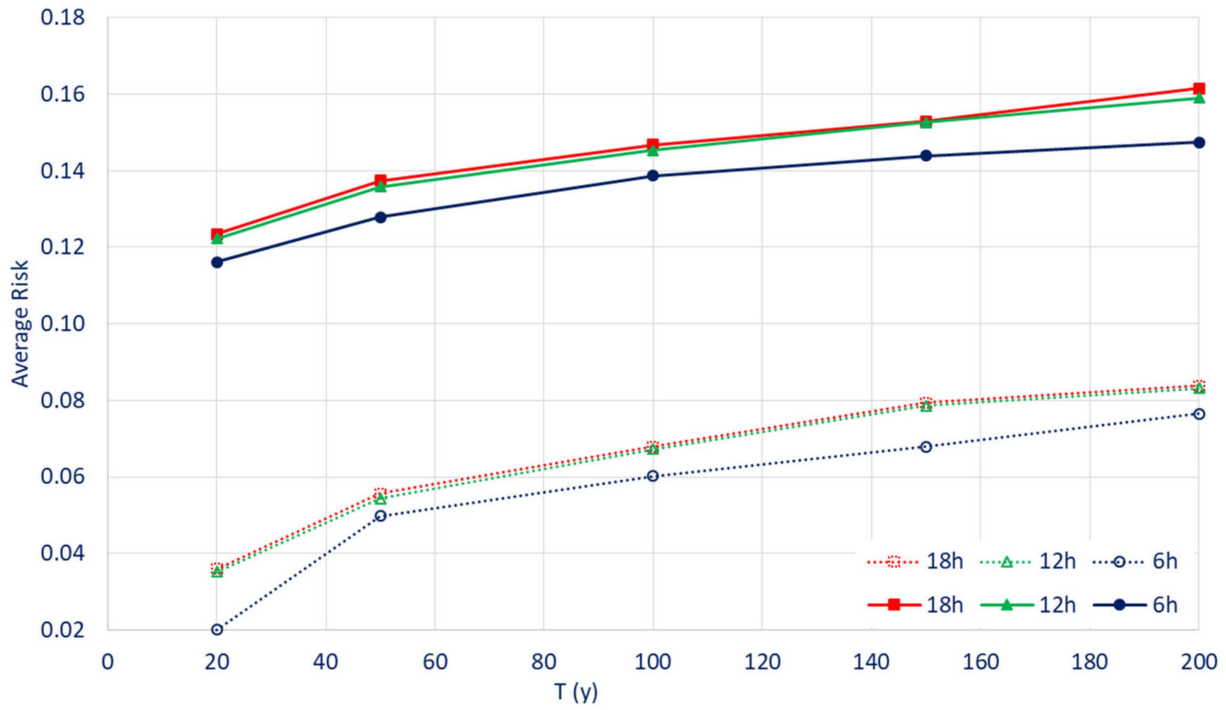
Figure 15. Relationship between the average risk and the flood return period (dotted lines represent scenarios with flood protection works).
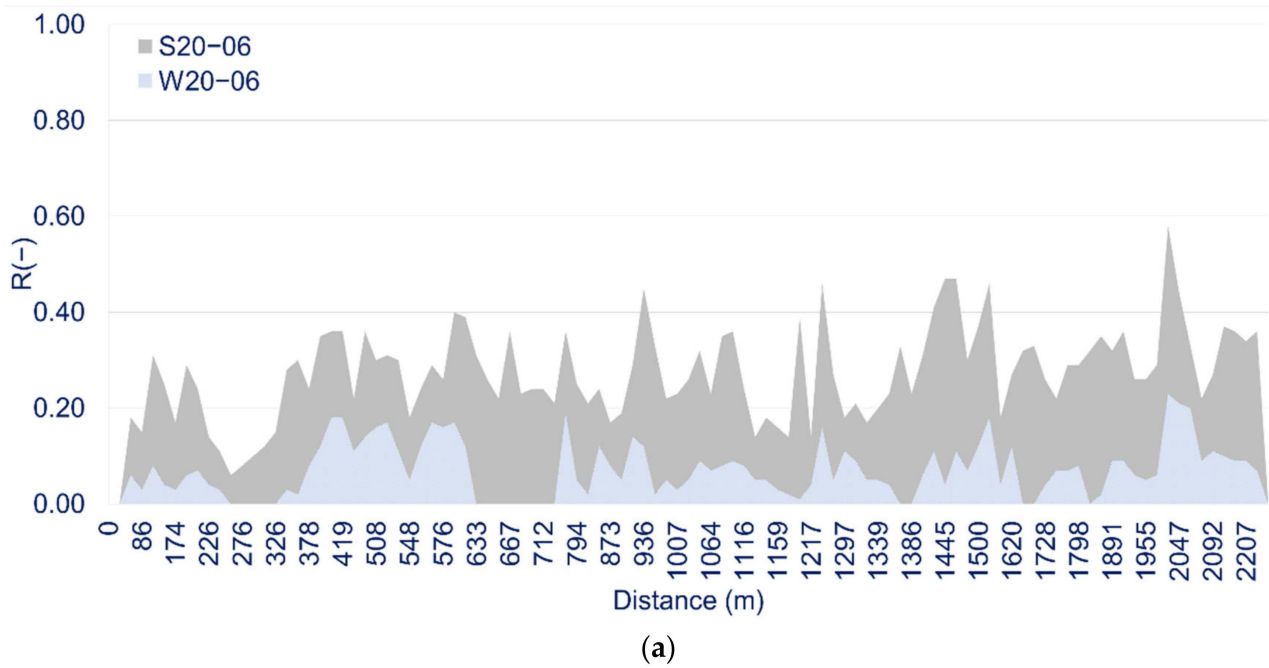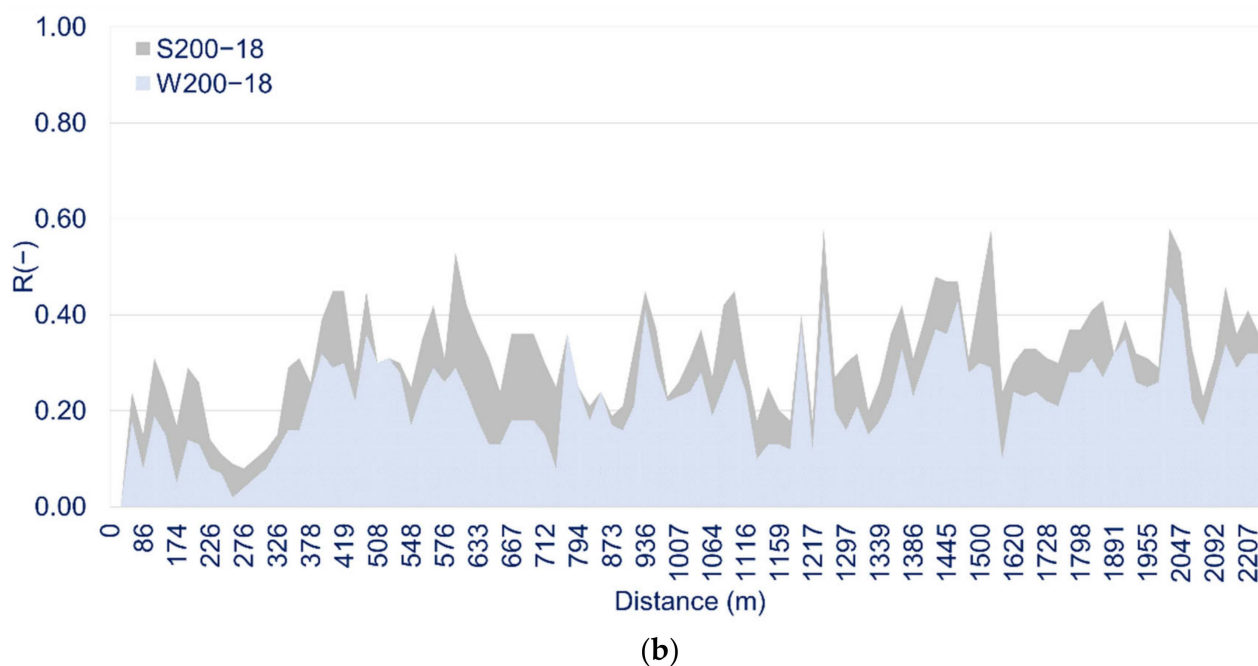

(**a**)

Figure 16. *Cont.*

(b)

Figure 16. Calculated flood risk along Koropouli Street for 4 indicative scenarios: (**a**) Scenarios S20-06 and W20-06 for T = 20 y and t = 6 h. (**b**) Scenarios S200-18 and W200-18 for T = 200 y and t = 18 h.

4. Discussion

This study explores the effects of flood protection works on the basis of hydrological and hydrodynamic model-derived calculations, using the town of Mandra in Greece as a case study. The study exploits a novel approach in assessing flood vulnerability in combination with flood hazard assessment to estimate the changes in flood risk under various rainfall and discharge scenarios. The findings illustrate a significant reduction in overall flood risk in the study area when scenarios with and without flood protection works are compared. In addition, the study presents a novel approach in estimating the overall risk by combining flood hazard assessment with flood vulnerability assessment on a building-by-building basis.

Examination of flood hazard shows a reduction in all indicators used in the present study (including flood extent, flow velocity, water depth, and average hazard), across the length of the flood plain examined, when the scenarios with flood protection works are employed. Similar findings are shown in the examination of the overall flood risk, with a clear reduction when flood protection works are present, across different scenarios of return period and duration. In all scenarios, the impacts decrease as the return period increases, indicating that the flood protection works in question are expected to have a more impressive effect on less extreme rather than more extreme storms.

Our results are consistent with the findings of previous studies [53,54]. Based on the concept of the disaster risk triangle (hazard, vulnerability, and exposure), a comprehensive analysis method and a general procedure were combined for urban flood risk analysis in China [54]. An urban flood simulation model and an urban flood damage assessment model were proposed for the estimation of the flood risk reduction due to flood control works in the Pudong flood protection area in Shanghai. Calculations showed that flood control works reduced the flood risk by 15.59% for the 66-year flood return period; however, for longer return periods, the flood risk reduction was only 7.06%. This conclusion is consistent with the findings of the present study, in which it was shown that the effect of flood protection works decreases with increasing return period and increasing rain duration. Moreover, in a recent study on the possible completion of a waterway from Padova to the Venice Lagoon, in Northeast Italy, it was shown that the use of the waterway as a flood

canal to divert part of the Brenta's floodwaters to the Venice Lagoon reduced the flood hazard in the downstream region of the Brenta and Bacchiglione Rivers. The effect of the waterway on flood risk reduction was tested by simulating several recent flood events characterized by important discharges in both the Brenta and Bacchiglione rivers [53].

In terms of practical implications, this study demonstrates a highly transferable approach that has the potential to provide an actual quantification of the benefit (if any) that such infrastructure has on flood hazard and flood risk, and to illustrate the changes in actual physical attributes of floodwaters, including depth, velocity, and extent. This is of particular importance in any cost–benefit analysis when planning for such flood protection interventions, for understanding how flood risk is expected to change depending on the type and characteristics of the planned works. Moreover, because of the visualization that it incorporates (i.e., flood extent or flood risk maps), the proposed approach can be a good communication tool, which is expected to be of interest to risk, insurance, and civil protection professionals, policymakers, and urban planning officials, as well as academics and engineers. The approach followed in this study can be applied in different parts of the world provided that the relevant data are available.

With regard to limitations, it must be noted that the differences calculated in depth, velocity, and flood extent are subject to assumptions that accompany the models used. In addition, the model predictions are subject to change depending on the condition of the channel and the hydraulic works. It is not rare to see accumulation of debris, vegetation, or vegetation fragments on bridge piers or at the entrances of drainage conduits [55], affecting the flow [56] or, in some extreme cases, blocking part of the channel or reducing its cross-sectional area [57,58]. Similar limitations should be noted for floodplain flow, as given the complexity of hydraulics in urban areas, changes—for example, in road infrastructure, new buildings, etc.—may result in diversion of flow in other parts of the floodplain or lead to differences in depth and velocity compared to what the model predicts based on the current conditions. Furthermore, it must be noted that the vulnerability estimation approach focuses on the susceptibility of buildings to internal flooding, excluding structural damages in the load-bearing structure. Future research could explore statistical relationships between construction materials and multiple criteria against flood impact to enrich the proposed approach. However, given the extensive similarities in construction methods and materials used in this case and in Greece in general due to strict building codes, there are expected to be only minor variations in vulnerability. In addition, there are various factors that affect the uncertainty of the calculated water depths, flow velocities, and inundation areas, which influence the calculation of flood hazard and risk. Some of the most important parameters include (a) the quality of the input data to the models, such as the geometric characteristics of the calculation domain, i.e., the DSM, the rainfall characteristics, and the values of the Manning roughness coefficients; (b) the assumptions that accompany the models, such as the simplifications made in the hydrodynamic equations—e.g., using the diffusion-wave equations—and the resolution of the computational grid; and (c) the methodologies adopted for the estimation of flood hazard and vulnerability [59]. To deal with these uncertainties, in the present work, we employed (a) the use of scenarios with various rainfall characteristics, and (b) the use of a hydrodynamic model that was calibrated [39] and optimized [19] via the use of the minimum required grid dimensions to combine fast computations and grid-independent results.

5. Conclusions

We developed a flood risk assessment method that combines the typical hazard assessment via integrated hydrological and hydrodynamic calculations using HEC-HMS and 1D/2D HEC-RAS, respectively, and an original procedure for vulnerability assessment at the building level, and we applied it in the town of Mandra in Attica, Greece.

We performed calculations for 15 scenarios—combinations of return periods (T = 20, 50, 100, 150, and 200 y) and rain durations (t = 6, 12, and 18 h)—for the conditions of the year 2017, when there were no flood protection works, and today with these works in place.

We identified the regions with high flood risk and concluded that the presence of the works resulted in a decrease in the expected inundation areas by a significant degree, i.e., 53–89% (for t = 18 h) and 56–93% (for t = 6 h). Moreover, we concluded that the maximum water depths, maximum flow velocities, and the average flood risk on Koropouli Street—which is the main street of Mandra and suffered severe damages during the 2017 flood—were expected to be reduced by 38–62%, 18–52%, and 27–74%, respectively. Average flood hazard values followed the same pattern, with an estimated reduction of 24–75% depending on the scenario (i.e., duration and return period). The effect of the flood protection works decreased with increasing return period and increasing rain duration, while for the same return period the effect of the rain duration was more pronounced for the smaller return periods. Overall, this study demonstrates a method that provides an actual quantification of the impact of flood protection works on flood risk in an urban environment. This approach could be followed elsewhere to improve the planning and development of such works, as well as to fine-tune policies and urban planning in post-development periods.

Author Contributions: Conceptualization, A.S., A.B., E.B. and G.M.; methodology, A.S., G.M., A.B., M.D., E.B., E.L.; software, G.M., A.B., M.D. and E.B; validation, X G.M., A.B., M.D. and E.B; formal analysis, G.M., A.B., M.D., A.S. and E.B; investigation, G.M., A.B., M.D., A.S. and E.L.; resources, E.B. and A.S.; data curation, G.M., M.D., A.B.; writing—original draft preparation, A.S., G.M., M.D., E.B., E.L. and A.B.; writing—review and editing, A.S., G.M., M.D., E.B. and A.B.; visualization, G.M., A.B. and M.D.; supervision, A.S. and E.L.; project administration, A.S.; All authors have read and agreed to the published version of the manuscript.

Institutional Review Board Statement: Not applicable.

Informed Consent Statement: Not applicable.

Data Availability Statement: Data available upon request.

Conflicts of Interest: The authors declare no conflict of interest.

References

1. Ulbrich, U.; Brücher, T.; Fink, A.H.; Leckebusch, G.C.; Krüger, A.; Pinto, J.G. The central European floods of August 2002: Part 1—Rainfall periods and flood development. *Weather* **2003**, *58*, 371–377. [CrossRef]
2. European Environment Agency. Deaths Related to Flooding in Europe. Available online: https://www.eea.europa.eu/data-and-maps/figures/people-per-million-population-affected-4 (accessed on 1 November 2022).
3. Cornwall, W. Europe's deadly floods leave scientists stunned. *Science* **2021**, *373*, 372–373. [CrossRef] [PubMed]
4. European Union Directive 2007/60/EC of the European Counil and European Parliment of 23 October 2007 on the assessment and management of flood risks. *Off. J. Eur. Union* **2007**, *288*, 27–34.
5. Merz, B.; Kreibich, H.; Thieken, A.; Schmidtke, R. Estimation uncertainty of direct monetary flood damage to buildings. *Nat. Hazards Earth Syst. Sci.* **2004**, *4*, 153–163. [CrossRef]
6. Pistrika, A.K.; Tsakiris, G. Flood risk assessment: A methodological framework. *Water Resour. Manag. New* **2007**, *1*, 14–16.
7. Diez-Herrero, A.; Garrote, J. Flood risk analysis and assessment, applications and uncertainties: A bibliometric review. *Water* **2020**, *12*, 2050. [CrossRef]
8. De Moel, H.; Jongman, B.; Kreibich, H.; Merz, B.; Penning-Rowsell, E.; Ward, P.J. Flood risk assessments at different spatial scales. *Mitig. Adapt. Strateg. Glob. Chang.* **2015**, *20*, 865–890. [CrossRef] [PubMed]
9. Wright, D.B. *Methods in Flood Hazard and Risk Assessment*; World Bank: New York, NY, USA, 2015.
10. Diakakis, M.; Deligiannakis, G.; Antoniadis, Z.; Melaki, M.; Katsetsiadou, N.K.; Andreadakis, E.; Spyrou, N.I.; Gogou, M. Proposal of a flash flood impact severity scale for the classification and mapping of flash flood impacts. *J. Hydrol.* **2020**, *590*, 125452. [CrossRef]
11. UNESCO-IHE. Flood Vulnerability Indices (FVI). Available online: http://www.unesco-ihe-fvi.org/ (accessed on 31 October 2022).
12. *IPCC Special Report: The Ocean and Cryosphere in a Changing Climate*; Cambridge University Press: Cambridge, UK, 2019.

13. Kappes, M.S.; Papathoma-Köhle, M.; Keiler, M. Assessing physical vulnerability for multi-hazards using an indicator-based methodology. *Appl. Geogr.* **2012**, *32*, 577–590. [CrossRef]

14. Connelly, A.; Carter, J.G.; Handley, J. State of the Art Report (4) Vulnerability Assessment: Definition, Indicators and Existing Assessment Methods. *Eur. Proj. RESIN–Clim. Resilient Cities Infrastruct.* **2015**, 12–50.

15. Kron, W. Flood risk = hazard ● values ● vulnerability. *Water Int.* **2005**, *30*, 58–68. [CrossRef]

16. Antony, R.; Rahiman, K.U.A.; Vishnudas, S. Flood Hazard Assessment and Flood Inundation Mapping—A Review. In *Current Trends in Civil Engineering: Select Proceedings of ICRACE 2020*; Thomas, J., Jayalekshmi, B.R., Praveen, N., Eds.; Springer: Singapore, 2020; pp. 209–219, ISBN 9789811581502.

17. Dung, N.B.; Long, N.Q.; Goyal, R.; An, D.T.; Minh, D.T. The Role of Factors Affecting Flood Hazard Zoning Using Analytical Hierarchy Process: A Review. *Earth Syst. Environ.* **2022**, *6*, 697–713. [CrossRef]

18. Munpa, P.; Kittipongvises, S.; Phetrak, A.; Sirichokchatchawan, W.; Taneepanichskul, N.; Lohwacharin, J.; Polprasert, C. Climatic and Hydrological Factors Affecting the Assessment of Flood Hazards and Resilience Using Modified UNDRR Indicators: Ayutthaya, Thailand. *Water* **2022**, *14*, 1603. [CrossRef]

19. Mitsopoulos, G.; Panagiotatou, E.; Sant, V.; Baltas, E.; Diakakis, M.; Lekkas, E.; Stamou, A. Optimizing the Performance of Coupled 1D/2D Hydrodynamic Models for Early Warning of Flash Floods. *Water* **2022**, *14*, 2356. [CrossRef]

20. Pita, G.L.; Albornoz, B.S.; Zaracho, J.I. Flood depth-damage and fragility functions derived with structured expert judgment. *J. Hydrol.* **2021**, *603*, 126982. [CrossRef]

21. Nixon, S. *EU Overview of Methodologies Used in Preparation of Flood Hazard and Flood Risk Maps*; EU Publications Office: Luxembourg, 2015.

22. Special Secretariat for Water. *Flood Risk Management Plan*; Special Secretariat for Water: Athens, Greece, 2015.

23. Custer, R.; Nishijima, K. *Flood Vulnerability Assessment of Residential Buildings by Explicit Damage Process Modelling*; Springer: Berlin/Heidelberg, Germany, 2015; Volume 78, ISBN 1106901517.

24. Papathoma-Köhle, M. Vulnerability curves vs. Vulnerability indicators: Application of an indicator-based methodology for debris-flow hazards. *Nat. Hazards Earth Syst. Sci.* **2016**, *16*, 1771–1790. [CrossRef]

25. Merz, B.; Kreibich, H.; Schwarze, R.; Thieken, A. Review article "Assessment of economic flood damage". *Nat. Hazards Earth Syst. Sci* **2010**, *10*, 1697–1724. [CrossRef]

26. Nasiri, H.; Yusof, M.J.M.; Ali, T.A.M.; Hussein, M.K.B. District flood vulnerability index: Urban decision-making tool. *Int. J. Environ. Sci. Technol.* **2019**, *16*, 2249–2258. [CrossRef]

27. UNDRR. Structural and Non-Structural Measures. Available online: https://www.undrr.org/terminology/structural-and-non-structural-measures (accessed on 1 November 2022).

28. Guo, Z.; Chen, L.; Yin, K.; Shrestha, D.P.; Zhang, L. Quantitative risk assessment of slow-moving landslides from the viewpoint of decision-making: A case study of the Three Gorges Reservoir in China. *Eng. Geol.* **2020**, *273*, 105667. [CrossRef]

29. Dong, X.; Guo, H.; Zeng, S. Enhancing future resilience in urban drainage system: Green versus grey infrastructure. *Water Res.* **2017**, *124*, 280–289. [CrossRef]

30. Panagiotatou, E.; Stamou, A. Mathematical Modelling of Nature-Based Solutions for flood risk reduction under Climate Change conditions. In Proceedings of the 7th IAHR Europe Congress, Athens, Greece, 7–9 September 2022; Stamou, A., Tsihrintzis, V., Eds.; IAHR: Athens, Greece, 2022.

31. Sayers, P.; Li, Y.; Galloway, G.; Penning-Rowsell, E.; Shen, F.; Wen, K.; Chen, Y.; Le Quesne, T. *Flood Risk Management*; UNESCO: Paris, France, 2013; ISBN 9781606921470.

32. Freni, G.; La Loggia, G.; Notaro, V. Uncertainty in urban flood damage assessment due to urban drainage modelling and depth-damage curve estimation. *Water Sci. Technol.* **2010**, *61*, 2979–2993. [CrossRef] [PubMed]

33. Diakakis, M.; Deligiannakis, G.; Andreadakis, E.; Katsetsiadou, K.N.; Spyrou, N.I.; Gogou, M.E. How different surrounding environments influence the characteristics of flash flood-mortality: The case of the 2017 extreme flood in Mandra, Greece. *J. Flood Risk Manag.* **2020**, *13*, e12613. [CrossRef]

34. Diakakis, M.; Andreadakis, E.; Nikolopoulos, E.I.; Spyrou, N.I.; Gogou, M.E.; Deligiannakis, G.; Katsetsiadou, N.K.; Antoniadis, Z.; Melaki, M.; Georgakopoulos, A.; et al. An integrated approach of ground and aerial observations in flash flood disaster investigations. The case of the 2017 Mandra flash flood in Greece. *Int. J. Disaster Risk Reduct.* **2019**, *33*, 290–309. [CrossRef]

35. Anastasios, S. The Disastrous Flash Flood of Mandra in Attica-Greece and now What? *Civ. Eng. Res. J.* **2018**, *6*, 1–6. [CrossRef]

36. IFRC. *Emergency Plan of Action Final Report Greece: Floods*; IFRC: Geneva, Switzerland, 2017.

37. Stamou, A.; Mitsopoulos, G.; Baltas, E. Identification of the weak points in the application of a methodology for the design of Flood Early Warning Systems in Cli-mate Change Conditions—The case of the town of Mandra. In Proceedings of the 7th IAHR Europe Congress, Athens, Greece, 7–9 September 2022; Stamou, A., Tsihrintzis, V., Eds.; IAHR: Athens, Greece, 2022.

38. (GSRI), G.S. of R. and I. Climpact: National Network for Climate Change and Its Impact. Available online: https://climpact.gr/ (accessed on 1 November 2022).

39. Mitsopoulos, G.; Diakakis, M.; Panagiotatou, E.; Sant, V.; Bloutsos, A.; Lekkas, E.; Baltas, E.; Stamou, A.I. 'How would an extreme flood have behaved if flood protection works were built?' the case of the disastrous flash flood of November 2017 in Mandra, Attica, Greece. *Urban Water J.* **2022**, *19*, 911–921. [CrossRef]

40. Feloni, E.; Theochari, A.-P.; Skroufouta, S.; Bournas, A.; Baltas, E. Analysis of the hydrologic conditions during the flood event occurred in Mandra, Greece, on November 2017. In Proceedings of the 17th International Conference on Environmental Science and Technology, Athens, Greece, 1–4 September 2021; CEST: Athens, Greece, 2021.

41. Brunner, G. *HEC-RAS River Analysis System Hydraulic Reference Manual Version 5.0*; Hydrologic Engineering Center, Institute for Water Resources, U.S. Army Corps of Engineers: Davis, CA, USA, 2016.

42. Bournas, A.; Baltas, E.; Stamou, A. Implementation of the Gridded Flash Flood Guidance Method in the Mandra Basin in west Attica, Greece. In Proceedings of the 7th IAHR Europe Congress: Innovative Water Management in a Changing Climate, Athens, Greece, 7–9 September 2022; Stamou, A., Tsihrintzis, V., Eds.; IAHR: Athens, Greece, 2022; Volume 1, pp. 457–458.

43. Bournas, A.; Baltas, E. Investigation of the gridded flash flood Guidance in a Peri-Urban basin in greater Athens area, Greece. *J. Hydrol.* **2022**, *610*, 127820. [CrossRef]

44. Neuhold, C.; Nachtnebel, H. Flood risk assessment in an Austrian municipality comprising the evaluation of effectiveness and efficiency of flood mitiga-tion measures. In *Flood Risk Management: Research and Practice*; Samuels, P., Huntington, S., Allsop, W., Harrop, J., Eds.; Routledge: London, UK, 2008; pp. 767–773.

45. Blanco-Vogt, A.; Schanze, J. Assessment of the physical flood susceptibility of buildings on a large scale–Conceptual and methodological frameworks. *Nat. Hazards Earth Syst. Sci.* **2014**, *14*, 2105–2117. [CrossRef]

46. BMVBS. *Hochwasserschutzfibel. Bauliche Schutz- und Vorsorgemaßnahmen in Hochwassergefährdeten Gebieten*; BMVBS: Berlin, Germany, 2006.

47. Fedeski, M.; Gwilliam, J. Urban sustainability in the presence of flood and geological hazards: The development of a GIS-based vulnerability and risk assessment methodology. *Landsc. Urban Plan.* **2007**, *83*, 50–61. [CrossRef]

48. Mazzorana, B.; Simoni, S.; Scherer, C.; Gems, B.; Fuchs, S.; Keiler, M. A physical approach on flood risk vulnerability of buildings. *Hydrol. Earth Syst. Sci.* **2014**, *18*, 3817–3836. [CrossRef]

49. Hawkesbury-Nepean Floodplain Management Steering Committee. Reducing Vulnerability of Buildings to Flood Damage. In *Guidance on Building in Flood Prone Areas*; Hawkesbury-Nepean Floodplain Management Steering Committee: Parramatta, Australia, 2006.

50. Müller, A.; Reiter, J.; Weiland, U. Assessment of urban vulnerability towards floods using an indicator-based approach—A case study for Santiago de Chile. *Nat. Hazards Earth Syst. Sci.* **2011**, *11*, 2107–2123. [CrossRef]

51. Diakakis, M.; Deligiannakis, G.; Pallikarakis, A.; Skordoulis, M. Identifying elements that affect the probability of buildings to suffer flooding in urban areas using Google Street View. A case study from Athens metropolitan area in Greece. *Int. J. Disaster Risk Reduct.* **2017**, *22*, 1–9. [CrossRef]

52. Apel, H.; Thieken, A.H.; Merz, B.; Blöschl, G. Natural Hazards and Earth System Sciences Flood risk assessment and associated uncertainty. *Nat. Hazards Earth Syst. Sci.* **2004**, *4*, 295–308. [CrossRef]

53. Mel, R.A.; Viero, D.P.; Carniello, L.; D'Alpaos, L. Multipurpose use of artificial channel networks for flood risk reduction: The case of the waterway Padova-Venice (Italy). *Water* **2020**, *12*, 1609. [CrossRef]

54. Li, C.; Cheng, X.; Li, N.; Du, X.; Yu, Q.; Kan, G. A framework for flood risk analysis and benefit assessment of flood control measures in Urban Areas. *Int. J. Environ. Res. Public Health* **2016**, *13*, 787. [CrossRef] [PubMed]

55. Thomas, H.; Nisbet, T. Modelling the hydraulic impact of reintroducing large woody debris into watercourses. *J. Flood Risk Manag.* **2012**, *5*, 164–174. [CrossRef]

56. Pagliara, S.; Carnacina, I. Bridge pier flow field in the presence of debris accumulation. *Proc. Inst. Civ. Eng. Water Manag.* **2013**, *166*, 187–198. [CrossRef]

57. Diakakis, M.; Boufidis, N.; Salanova Grau, J.M.; Andreadakis, E.; Stamos, I. A systematic assessment of the effects of extreme flash floods on transportation infrastructure and circulation: The example of the 2017 Mandra flood. *Int. J. Disaster Risk Reduct.* **2020**, *47*, 101542. [CrossRef]

58. Panici, D.; Kripakaran, P.; Djordjević, S.; Dentith, K. A practical method to assess risks from large wood debris accumulations at bridge piers. *Sci. Total Environ.* **2020**, *728*, 1–10. [CrossRef]

59. Pinheiro, V.B.; Naghettini, M.; Palmier, L.R. Uncertainty estimation in hydrodynamic modeling using Bayesian techniques. *Rev. Bras. Recur. Hidricos* **2019**, *24*, e38. [CrossRef]